Journal of Colloid and Interface Science 462 (2016) 252–259

Contents lists available at ScienceDirect

Journal of Colloid and Interface Science

journal homepage: www.elsevier.com/locate/jcis

The effect of pH on the adsorption of arsenic(III) and arsenic(V) at the TiO_2 anatase [1 0 1] surface

Zhigang Wei [a,*], Kai Liang [a], Yang Wu [b], Yandi Zou [a], Junhui Zuo [a], Diego Cortés Arriagada [c], Zhanchang Pan [a], Guanghui Hu [a]

[a] School of Chemical Engineering and Light Industry, Guangdong University of Technology, Guangzhou 510006, PR China
[b] College of Chemistry, Liaoning University, Shenyang 110036, PR China
[c] Laboratorio de Química Teórica-Computacional, Departamento de Química-Física, Pontificia Universidad Católica de Chile, Chile

GRAPHICAL ABSTRACT

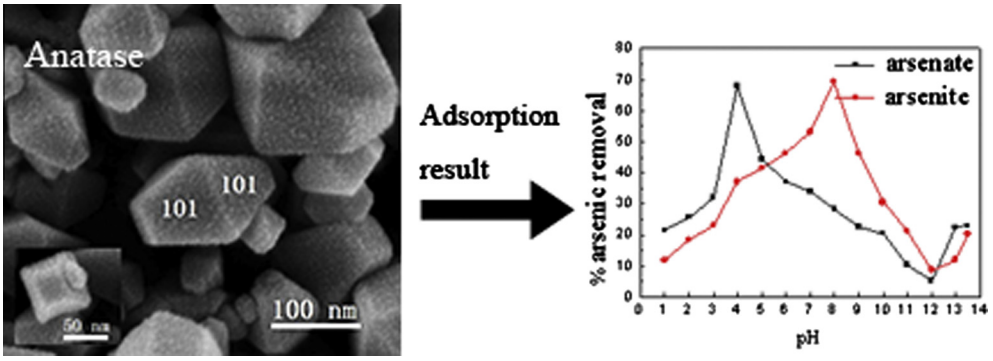

ARTICLE INFO

Article history:
Received 27 August 2015
Accepted 6 October 2015

Keywords:
Arsenate
Arsenite
TiO_2
Density functional theory
Adsorption

ABSTRACT

Octahedral TiO_2 nanocrystals (OTNs) have been prepared by a hydrothermal method with the main surface of (1 0 1). Then the arsenic adsorption behavior on OTNs is investigated in a broad experimental pH range from 1.0 to 13.5. The maximum adsorptions of arsenite (As(III)) and arsenate (As(V)) appear at pH values 8 and 4, respectively. It is interesting to see that the minimum adsorptions of As(III) and As(V) are both at pH 12 and then their adsorptions increase again at higher pH values such as 13.0 and 13.5. To our best knowledge, it is quite new to report the arsenic adsorption on the controlled TiO_2 surface especially at very high pH values. These results might be helpful to understand the adsorption mechanism. On the other hand, periodic slab models of TiO_2 anatase (1 0 1) surface with some H^+ cations, some water molecules or some OH^- ions are suggested to simulate the pH effect. Using these models, the adsorptions of As (III) and As(V) are simulated by the density functional theory (DFT) method. Qualitatively, the adsorption abilities of arsenic species, water and OH^- follow the order of $AsO_3^{3-} > OH^- > HAsO_3^{2-} > H_2AsO_3^- > H_2O > H_3AsO_3$ for As(III) and $AsO_4^{3-} > OH^- > HAsO_4^{2-} > H_2AsO_4^- > H_3AsO_4 > H_2O$ for As(V). It implies that $H_2AsO_3^-$ should be the major As(III) species at pH 8 and $H_2AsO_4^-$ should be the major As (V) species at pH 4, and the most negative charged ions AsO_3^{3-} and AsO_4^{3-} should correspond to the adsorptions at the high pH values 13 and 13.5.

* Corresponding author.
E-mail address: weizg2003@126.com (Z. Wei).

http://dx.doi.org/10.1016/j.jcis.2015.10.018
0021-9797/

1. Introduction

As a cheap and nontoxic material, TiO_2 has been extensively used for arsenic removal due to the strong sorption of As(III) and As(V) on it [1,2]. Some investigations were carried out by different groups and similar conclusions were obtained that the max adsorption pH for As(III) was near 9 and the max adsorption pH for As(V) was near 4 [3–8]. Two kinds of adsorption mechanisms have been suggested based on the models of electrostatic factors and surface complexes [3]. These results and conclusions are very useful. However, some improvements are still needed both from experiments and from the adsorption models to deeply understand the adsorption mechanism.

It is known that the (1 0 1) surface is the most abundant surface for anatase in nature. During previous experiments, when they could not control the surface to be (1 0 1), it was difficult to exclude or evaluate the interferences from other surfaces. In addition, due to the neutral pH of the usually used water, most investigations were focused on the pH range from 4 to 9. However, the minimum adsorption at high pH value is important for TiO_2 regeneration process. In the present paper, the (1 0 1) surface has been controlled during the powder synthesis and a broad experimental pH range of 1.0–13.5 is tested to show whether the surface control has a profound influence on the pH effect.

The adsorption mechanism in some sense is more complex to discuss because different distributions of As(III) and As(V) exist in water solution as a function of pH such as in Eqs. (1)–(3) [3,9] and Eqs. (4)–(6) [3,9,10] at 25 °C.

$$H_3AsO_3 \leftrightarrow H^+ + H_2AsO_3^- \quad pK_1 = 9.23 \tag{1}$$

$$H_2AsO_3^- \leftrightarrow H^+ + HAsO_3^{2-} \quad pK_2 = 12.10 \tag{2}$$

$$HAsO_3^{2-} \leftrightarrow H^+ + AsO_3^{3-} \quad pK_3 = 13.41 \tag{3}$$

$$H_3AsO_4 \leftrightarrow H^+ + H_2AsO_4^- \quad pK_1 = 2.3 \tag{4}$$

$$H_2AsO_4^- \leftrightarrow H^+ + HAsO_4^{2-} \quad pK_2 = 6.8 \tag{5}$$

$$HAsO_4^{2-} \leftrightarrow H^+ + AsO_4^{3-} \quad pK_3 = 11.6 \tag{6}$$

Therefore, different kinds of arsenic species might appear on the surface at different pH range. The main question is whether the main species in the solution would be the main one on the surface, and how the surface complex changes with pH. In the present paper, a new attempt is made to explain the adsorption mechanism based on the DFT calculations with periodic slab models. The next section gives details about the experimental and computational methods. The results section examines the adsorption behavior of arsenic on TiO_2 anatase (1 0 1) surface at pH range of 1.0–13.5 and a comparison between previous experimental results is made. Then the DFT calculation results are shown to explain the adsorption mechanism and the most favorable adsorption species and structures are suggested. At last, a brief summary is made and some conclusions are given.

2. Experimental and computational methods

2.1. Sample preparation and characterization

Octahedral TiO_2 nanocrystals (OTNs) are prepared by a hydrothermal method [11]. 1 g of P25 is added into 10 M KOH solution. After 1 h ultrasonic dispersion uniformity, the turbid liquid is transferred into a 60 mL Teflon-lined autoclave, heated at 200 °C for 24 h, and then is naturally cooled to room temperature. The producing white precipitates are centrifuged and washed thoroughly with deionized water. Subsequently, the white precipitates are immerged into a 0.1 M NH_4NO_3 solution for 12 h, washed with deionized water and then dried at 60 °C for 10 h. The proper obtained precursors with 0.05 M hexamethylenetetramine are placed into a 60 mL Teflon-lined autoclave and heated at 200 °C for 24 h. Finally, the OTNs are isolated from solution by centrifugation and dried at 60 °C for 10 h. The obtained OTNs are removed organic compounds by heated at 350 °C.

OTNs are determined by a powder X-ray diffractometry (XRD, Rigaku-Ultima III with Cu Kα radiation). Scanning electron microscopy (SEM) is recorded on a field-emission scanning electron microscopy (FE-SEM, Hitachi S-4800). Specific surface areas (S_{BET}) and pore distribution of adsorbents are measured by Brunauere–Emmette–Teller N_2 adsorption–desorption on a Micromeritics ASAP 2020 Analyzer.

Stock solutions containing 100 mg L^{-1} of arsenic are prepared by dissolving As_2O_3 in redistilled water containing 0.1% (w/w) NaOH and $Na_3AsO_4{\cdot}12H_2O$ in redistilled water. The arsenic concentrations are determined with a rapid colorimetric method [12]. All chemicals used in the experiments are analytical grade and all the solutions are prepared with the redistilled water. It should be noted that all adsorption experiments are carried out for three times.

2.2. Computational method

The calculations are performed with DFT in periodic slab models [13]. Atomic basis sets are applied numerically in terms of a double numerical plus polarization function [14] and a global orbital cutoff of 5.2 Å is employed. The exchange–correlation interaction is treated within the generalized gradient approximation (GGA) with the functional parameterized by Perdew, Burke and Enzerhof (PBE) [15]. The spin-polarization effects are also included in the calculations for the open-shell systems. The system charges are used for the charged systems [16,17]. The conductor-like screening model (COSMO) [18,19] is applied to simulate the water solvent environment using a dielectric constant of 78.54 appropriate to water at 25 °C. All electron DFT calculations are performed using a DMol3 package [20–22] in Materials Studio.

3. Results and discussion

3.1. Structure and morphology

Fig. 1 shows the XRD patterns of obtained precursors and OTNs. The sharp diffraction peaks of OTNs match clearly with the crystal structure of the anatase TiO_2 phase (tetragonal, $I4_1/amd$,

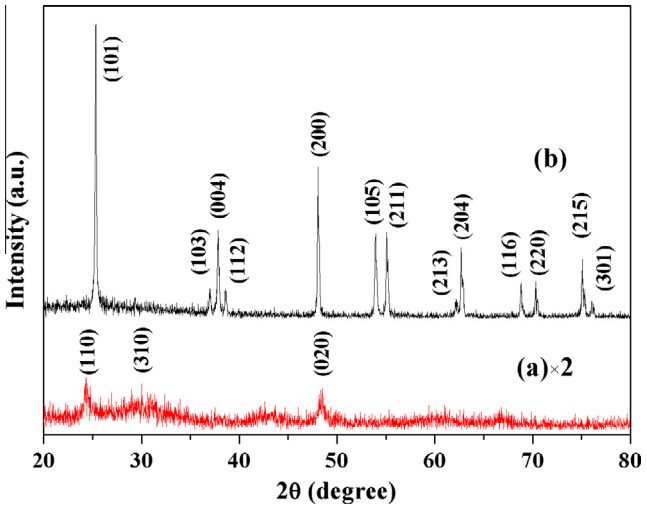

Fig. 1. X-ray diffraction patterns: (a) OTNs precursors and (b) the OTNs products.

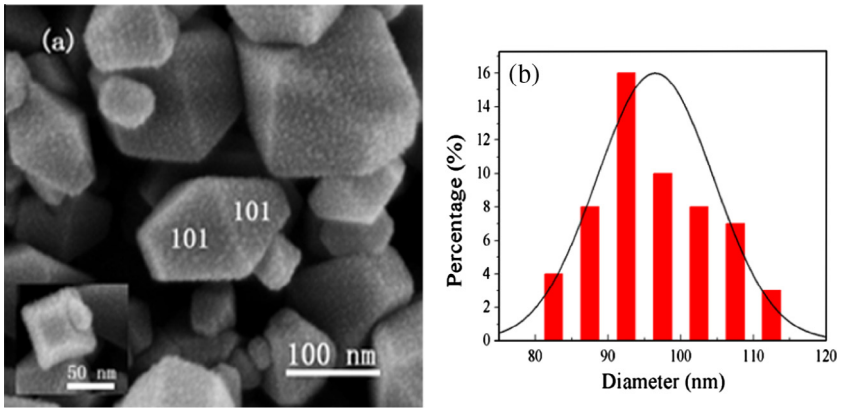

Fig. 2. (a) Higher SEM image of OTNs and (b) statistical analyses of OTNs particles diameters. The inset of (a) is the top view of a single OTNs.

JCPDS 21-1272), indicating pure and perfect crystallographic structure is observed. Fig. 2(a) shows a higher SEM image of OTNs with octahedral bipyramid morphology. All the OTNs perform well-defined lateral crystal face (predominantly anatase 101 facet) with sharp edges and adjacent crystal faces are vertical as well as with the same width (inset of Fig. 2(a)). Fig. 2(b) shows the particle diameter statistical histogram of OTNs, and the average size 96.34 nm is calculated from measuring the diameter of stochastic 100 OTNs. The specific surface area of OTNs measured by BET is 17.6 $m^2 g^{-1}$.

3.2. Adsorption equilibrium time

The experiments are performed in air-dark systems and the suspensions are prepared in 0.5-L glass beakers. Aliquots of As(III) and As(V) stock solutions are added to make 0.2 mg L^{-1} of As(III) or As (V) concentration. After adjusting the pH of solutions to the desired values such as 4, 7 and 9 by adding hydrochloric acid and sodium hydroxide, TiO_2 is added to attain a 0.1 g L^{-1} suspension. Then the 0.5 L suspensions are sealed and stirred by magnetic stirrer at room temperature. As shown in Fig. 3, As(III) and As(V) adsorption equilibria at various pH are established in approximately 90 and 150 min, respectively. We have kept the adsorption overnight but the results do not change (see Fig. 1s in the appendix).

3.3. Effect of pH on arsenic adsorption

To a deeper understanding of the pH effect, a systemic study has been carried out for all the possible pH values such as 1, 2, 3, . . . 13, 13.5. The instruments and operating steps are the same as described in Section 3.2. The removals of As(III) and As(V) by TiO_2 adsorbent are shown in Fig. 4. It shows that the adsorption of As(III) increases from 11% to 70% when the solution pH increases from 1 to 8, then decreases from 70% to 8% for pH from 8 to 12, finally increases to 11% and 20% for pH values 13 and 13.5, respectively. Fig. 4 also illustrates that the maximum adsorption of As(V) appeares at pH 4 and the maximum adsorption ratio is 68%, then there is a decrease from pH 4 to pH 1. On the other side, there is a large decrease from pH 4 to pH 12, and the adsorption ratio at the minimum point is only about 5%. Then, there is a rise from pH 12 to 13.5 with an adsorption ratio increase from 5% to 22%. It should be noted here that the adsorption increase from pH 12 to 13.5 for both As(III) and As(V) should correspond to some changes for the adsorption mechanism that has not yet been clearly observed and understood.

3.4. Comparing with previous experimental results

There have been some experiments about arsenic adsorption on TiO_2 anatase surface [3–8], as collected in Table 1. It is clear that all

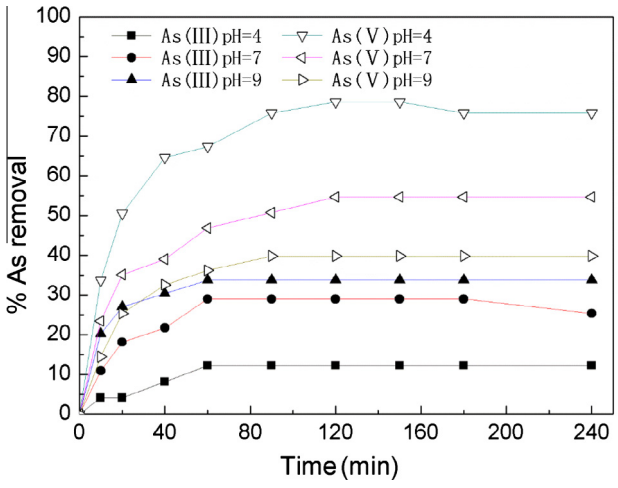

Fig. 3. Adsorption equilibrium of arsenic removal by OTNs adsorbent. Initial As(III) = As(V) = 0.200 mg L^{-1}; OTNs content = 0.1 g L^{-1}; solution pH values were 4, 7 and 9.

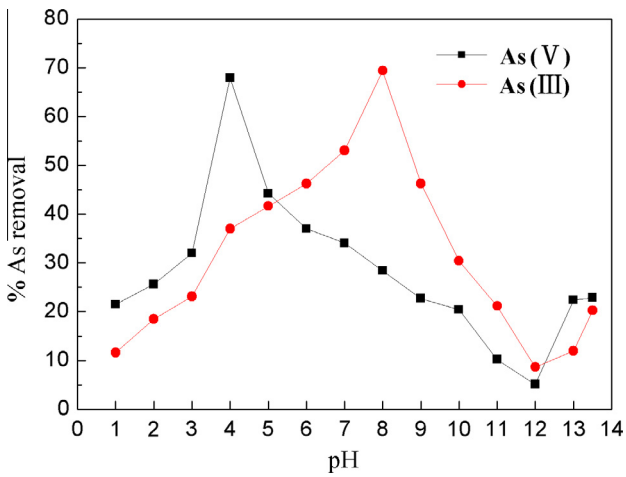

Fig. 4. Removal of arsenic as a function of solution pH in a suspension containing 0.2 mg L^{-1} of arsenic and 0.1 g L^{-1} of OTNs.

Table 1
A comparison of the physicochemical properties of TiO_2 anatase samples and their adsorption properties.

	This work	Ref. [3]	Ref. [5,6]	Ref. [4]	Ref. [7]	Ref. [8]
Particle size (μm)	0.08–0.11	<0.010	0.5–2	150–600	–	0.108
S_{BET} ($m^2\ g^{-1}$)	17.6	334	330	250.7	98.3	–
$C_{As(III)}$ ($mg\ L^{-1}$)	0.200	10	1.0	0.300	1	5
$C_{As(V)}$ ($mg\ L^{-1}$)	0.200	10	1.0	0.300	1	5
C_{TiO2} ($g\ L^{-1}$)	0.1	–	0.2	0.3; 0.6; 1.0	0.2	1
$V_{suspension}$ (L)	0.5	–	0.05	0.1	–	0.25
Mixed time (h)	4	2	22	2 for As(V) 5 for As(III)	72	24
pH rang	1–13.5	3–9	4–13	4–11	3–11	1–14
Water resource	Redistilled water	Ultra pure water	Deionized water	Ground water	–	Deionized water
Max adsorption pH for As(III)	8	–	9	8.5	9	7
Min adsorption pH for As(III)	12	–	–	–	–	14
Max adsorption pH for As(V)	4	3	5	4	6	1–5
Min adsorption pH for As(V)	12	9	–	–	–	14
pH_{PZC}	–	6.2	5.8	–	4.8	–

the experiments were carried out at similar processes and conditions except for different TiO_2 particle size, S_{BET}, arsenic and TiO_2 concentrations, etc. It should be noted that the (101) surface, which is the most thermodynamically stable surface, should also be the most abundant surface in the previous papers. As shown in Fig. 4, our results are in agreement with the previous results during pH 4–9 for As(V) and during pH 3–11 for As(III). Especially, the maximum and minimum adsorption pH values for arsenic can be clearly observed in Fig. 4. The maximum adsorption pH value for As(III) is at pH 8, which is only a little lower than the previous results (pH 8.5 or 9) as listed in Table 1. All the previous reports showed that the adsorption ability of As(III) became lower on both sides of the maximum adsorption pH value. The same trend can be found in Fig. 4. The most notable difference with respect to our data is that the minimum value at high pH of 12. To our knowledge, only Pena et al. [5] and Nabi et al. [8] reported about the adsorption of As(III) at pH values higher than 12. For Pena et al. [5], an adsorption minimum for As(III) at pH 12 was given for the dark system in their challenge water, whereas in their deionized water experiments the adsorption minimum disappeared. Nabi et al. [8] reported that the adsorption decreased from pH 7 to pH 14. For a detail comparison, the arsenic concentrations of Pena et al. [5] and Nabi et al. [8] were 5 times and 25 times higher respectively than that in the present paper, and at the same time the concentrations of TiO_2 were 2 and 10 times higher respectively than that in the present paper. Furthermore, the surface area 17.6 $m^2\ g^{-1}$ in the present paper is much lower than that of 330 $m^2\ g^{-1}$ from Pena et al. [5]. Therefore, there should be strong particle size effect and arsenic concentration effect between our results and their results.

Compared to As(III), the effect of pH on As(V) sorption is more pronounced. Although many researches did not obtain the maximum adsorption pH values for As(V), they all agreed that acidic condition were helpful for the adsorption of As(V). Dutta et al. [3] suggested that the maximum and minimum adsorption pH values for As(V) were 3 and 9, although the pH range in their paper was only from 3 to 9. Nabi et al. [8] reported that the adsorption decreased from pH 7 to pH 14. In the present paper, the maximum and minimum adsorption pH values are 4 and 12 as shown in Fig. 4. Further work about the size, concentration and temperature effects is still desirable for this system.

3.5. The adsorption mechanism

In 2004, Dutta et al. suggested two models [3]. The first one was the electrostatic factors based on crystal pH_{pzc}. For examples, at pH 4 the crystal possesses positive charge and As(V) ($H_2AsO_4^-$) possesses negative charge, thus the adsorption is good; at pH 9 the crystal possesses negative charge and As(V) ($HAsO_4^{2-}$) also possesses negative charge, thus the adsorption is bad. Whereas this model did not fit well with As(III). Because the maximum adsorption is near pH 9 when the crystal possesses negative charge and the As(III) possesses approximately equimolar mixture of H_3AsO_3 and $H_2AsO_3^-$ in the solution. Therefore, Dutta et al. suggested the formation of surface complexes, which might vary with pH.

The electrostatic factors between the TiO_2 surface and arsenic species should be the basic reason for the strong adsorption of arsenic. However, pH_{PZC} (the pH for the point of zero charge) is corresponding to the whole crystal, while the adsorption process is a microcosmic process mainly between arsenic and surface, i.e., the surface Ti_{5c} (the 5 coordinates Ti) with positive charge would attract O atom of arsenic species and surface O_{2c} (the 2 coordinates O) with negative charge would attract H atom of arsenic species. So, microcosmic models are more desirable to describe arsenic adsorption. Basically there are two kinds of models used such as the cluster model [23,24] and the periodic slab model [25]. Simple sketches for the cluster model and the periodic slab model are shown in Figs. 2s and 3s in the appendix.

In 2009, Pan et al. [26] simulated the pH effect of As(V) through changing the number of H^+ with a cluster model similar to Fig. 2s. Based on the results of the adsorption energy, the bidentate binuclear (BB) surface complex was the most thermodynamically favorable mode (244.5 kJ mol^{-1}, i.e., 58.4 Kcal mol^{-1}) at low pH, but MM surface complex was the most thermodynamically favorable mode (135.6–27.5 kJ mol^{-1}, i.e., 32.4–6.6 Kcal mol^{-1}) at intermediate and high pH. In 2011, Pan et al. [27] simulated the pathway from the reactant complex (0.0 Kcal mol^{-1}) to the monodentate mononuclear (MM) surface configuration (−9.2 Kcal mol^{-1}) and then to the BB surface configuration (−16.7 Kcal mol^{-1}) in Fig. 4 of that paper. However, all these calculations only considered $H_2AsO_4^-$. For broad pH range and from Eqs. (4)–(6), all the As(V) species such as H_3AsO_4, $H_2AsO_4^-$, $HAsO_4^{2-}$, AsO_4^{3-} might appear and change to each other both in the solution and on the surface, and the adsorption and desorption might be reversible. In the models of Pan et al. [26,27] the total charge of the clusters were all positive such as $H_2AsO_4^-(H_2O)_{12} + [Ti_2(OH)_4(H_2O)_6]^{4+}$ for the low pH, $H_2AsO_4^-(H_2O)_{12} + [Ti_2(OH)_5(H_2O)_5]^{3+}$ for intermediate pH and $H_2AsO_4^-(H_2O)_{12} + [Ti_2(OH)_6(H_2O)_6]^{2+}$ for the high pH. In our point of view, all these models belong to low pH range. In addition, one weakness of the cluster model is that it cannot simulate the spatial extent of the real surface when Fig. 2s compares with Fig. 3s. As a result, the cluster model can only simulate the Ti_{5c} on the surface, but it cannot simulate the O_{2c} on the surface, therefore it cannot simulate the surface functional groups and surface complexes accurately.

In the recent years, we tried to simulate the arsenic-TiO_2 system by the periodic slab model [13,28,29]. In our previous papers [28,29], all the species of As(III) and As(V) with the BB and MM structures were considered and calculated. The adsorption orders

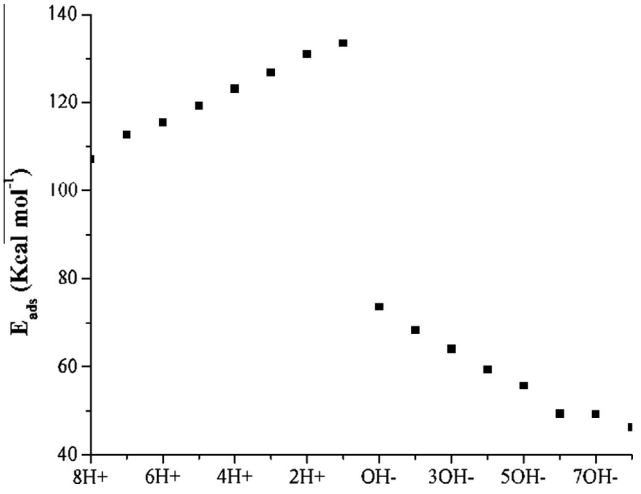

Fig. 5. The E_{ads} values of H^+ cations or OH^- ions on the surface, i.e., 8 H^+, 7 H^+, 6 H^+, 5 H^+, 4 H^+, 3 H^+, 2 H^+, H^+, OH^-, 2 OH^-, 3 OH^-, 4 OH^-, 5 OH^-, 6 OH^-, 7 OH^-, 8 OH^-.

of As(III) and As(V) were $OH^- > AsO_3^{3-} > HAsO_3^{2-} > H_2AsO_3^- > H_2O > H_3AsO_3$ and $OH^- > AsO_4^{3-} > HAsO_4^{2-} > H_2AsO_4^- > H_3AsO_4 > H_2O$, respectively. Thus, at high pH values OH^- would be more favorable on the surface than As(III) and As(V) species. But this conclusion cannot agree with the experimental results in the present paper such that there are minimum adsorption points at about pH 12 for both As(III) and As(V).

In the present paper, some improvements have been made in that model ($Ti_{32}O_{64}$ super cell) as shown in Fig. 3s. The arsenic complexes are adsorbed on the upper surface only, and the adsorption energy (in the supercell) is calculated as follows:

$$E_{ads} = E_{arsenic} + E_{surface} - E_{arsenic/surface} \quad (7)$$

where $E_{arsenic}$ and $E_{surface}$ are the energies of an isolated arsenic species and the surface respectively, and $E_{arsenic/surface}$ is the total energy of the same arsenic species adsorbed on the same surface. It should be mentioned that other E_{ads} are calculated by the same way such as water, H^+, and OH^-.

After these changes, a series of calculations are performed in order to ascertain whether the model could simulate the pH effect.

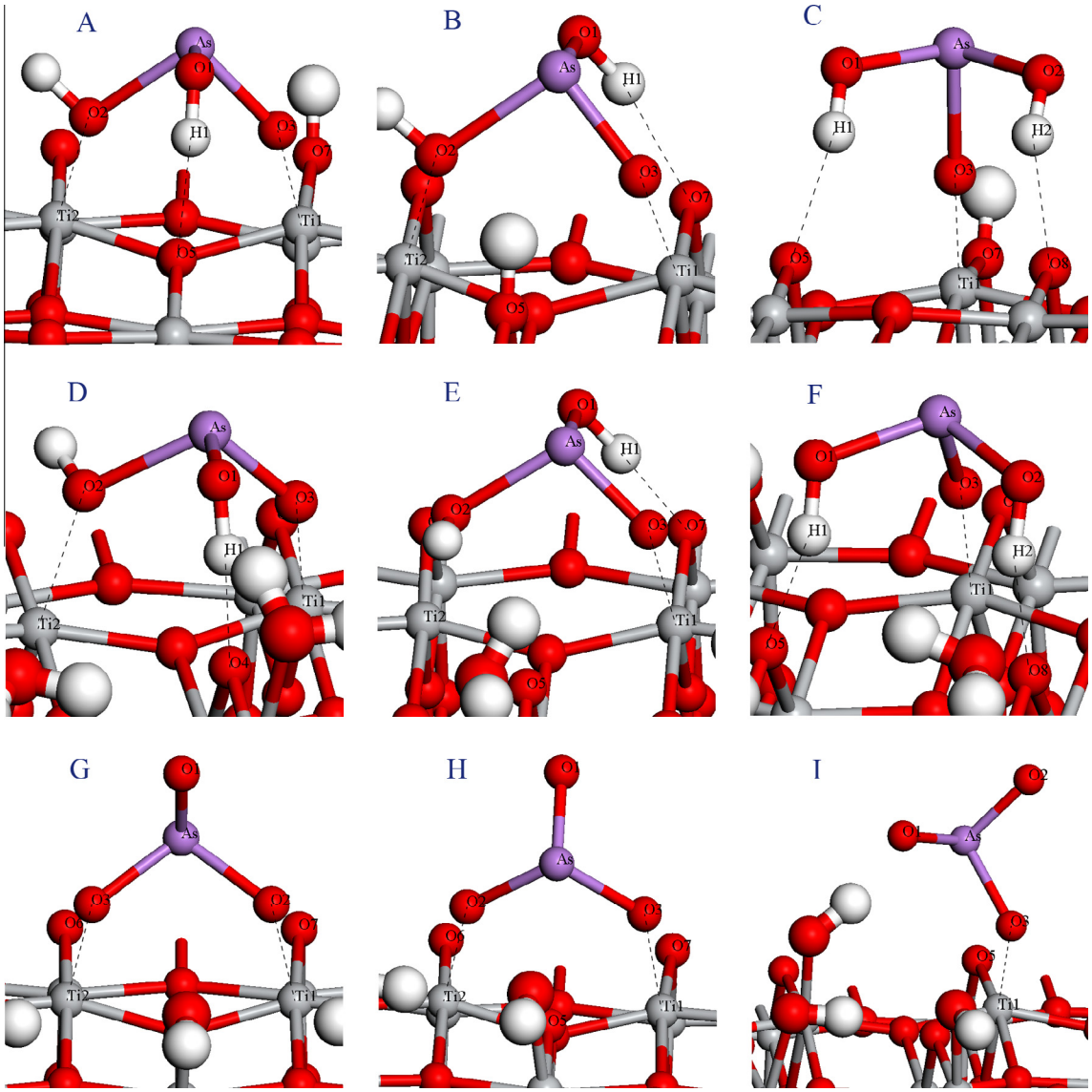

Fig. 6. The optimized As(III) geometries on TiO_2 anatase (1 0 1) surface (A–C at acidic condition; D–F at neutral condition; G–I at alkaline condition). (A) TiO_2-$H_2AsO_3^-$-1; (B) TiO_2-$H_2AsO_3^-$-2; (C) TiO_2-$H_2AsO_3^-$-3; (D) TiO_2-$H_2AsO_3^-$-1; (E) TiO_2-$H_2AsO_3^-$-2; (F) TiO_2-$H_2AsO_3^-$-3; (G) TiO_2-AsO_3^{3-}-1; (H) TiO_2-AsO_3^{3-}-2; and (I) TiO_2-AsO_3^{3-}-3.

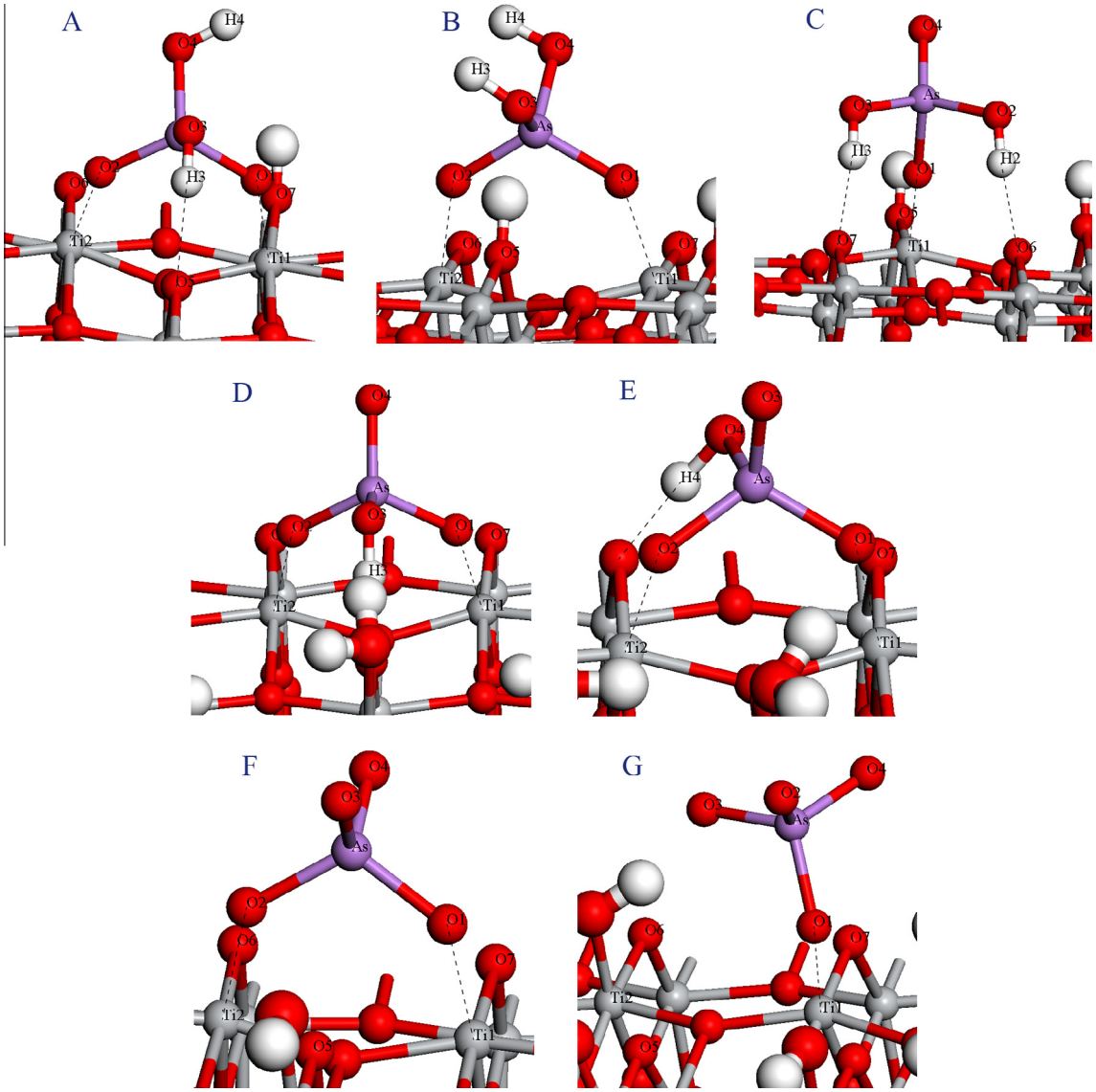

Fig. 7. The optimized As(V) geometries on TiO_2 anatase (1 0 1) surface (A–C at acidic condition; D–E at neutral condition; F–G at alkaline condition). (A) TiO_2-$H_2AsO_4^-$-1; (B) TiO_2-$H_2AsO_4^-$-2; (C) TiO_2-$H_2AsO_4^-$-3; (D) TiO_2-$HAsO_4^{2-}$-1; (E) TiO_2-$HAsO_4^{2-}$-2; (F) TiO_2-AsO_4^{3-}-1; and (G) TiO_2-AsO_4^{3-}-2.

In Fig. 5, the calculation E_{ads} results from the lowest pH (from eight H^+ cations on the surface to one H^+ cation on the surface) to the highest pH (from one OH^- ion to eight OH^- ions) are given. The linear relation of E_{ads} in Fig. 5 implies that this simple model, though heavily approximated, may give us useful information to explain the experimental results for the pH effect. Although it is difficult to give a clear function, there should be some relations between E_{ads} in Fig. 5 and the zeta potential of the TiO_2 particle such as in Fig. 1 from Dutta et al. [3]. From Fig. 5, it is clear that the E_{ads} of a single H^+ decreases from one H^+ to eight H^+, whereas the total E_{ads} of all the H^+ cations would increases. Therefore, there should be a large positive zeta potential for eight H^+ cations, i.e., at low pH value. On the other hand, the changing of the zeta potential should be slower at low pH values because the decrease of E_{ads} for a single H^+. The similar trend can be found for OH^- such as the large negative zeta potentials at high pH values and the slower changing of the zeta potential at high pH values. From Fig. 5 the larger E_{ads} of H^+ (133.5 kcal mol^{-1}) than that of OH^- (73.6 kcal mol^{-1}) agrees with the pH_{pzc} at 6.2 in Fig. 1 from Dutta et al. [3].

Table 2
The optimized geometries (Å) and E_{ads} of As(III) adsorption configurations on TiO_2 anatase (1 0 1) surface at acidic, neutral and alkaline pH conditions.

Species	As-O1	As-O2	As-O3	As-Ti1	As-Ti2	E_{ads}
TiO_2–$H_2AsO_3^-$-1[a]	1.776	1.996	1.856	3.507	3.814	80.2
TiO_2–$H_2AsO_3^-$-2[a]	1.784	2.048	1.821	3.395	3.734	76.1
TiO_2–$H_2AsO_3^-$-3[a]	1.804	1.803	1.952	3.671	–	69.9
TiO_2–$H_2AsO_3^-$-1[b]	1.810	1.973	1.772	3.528	3.888	31.1
TiO_2–$H_2AsO_3^-$-2[b]	1.831	1.996	1.766	3.410	3.778	37.8
TiO_2–$H_2AsO_3^-$-3[b]	1.846	1.849	1.788	3.623	–	41.2
TiO_2–AsO_3^{3-}-1[c]	1.751	1.868	1.865	3.322	3.319	90.9
TiO_2–AsO_3^{3-}-2[c]	1.748	1.859	1.866	3.504	3.507	90.7
TiO_2–AsO_3^{3-}-3[c]	1.781	1.762	1.940	3.333	–	82.2

[a] At acidic pH condition.
[b] At neutral pH condition.
[c] At alkaline pH condition.

Using this model and Eq. (7), six water molecules, six H^+ cations and six OH^- ions are put on the surface to qualitatively simulate the neutral pH, the acidic pH and the alkaline pH conditions, respectively. The adsorption structures and energies are shown in

Table 3
The optimized geometries (Å) and E_{ads} (kcal mol^{-1}) of As(V) adsorption configurations on TiO_2 anatase (1 0 1) surface at acidic, neutral and alkaline pH conditions.

Species	As-O1	As-O2	As-O3	As-O4	As-Ti1	As-Ti2	E_{ads}
TiO_2–$H_2AsO_4^-$-1[a]	1.749	1.718	1.747	1.737	3.364	3.396	69.8
TiO_2–$H_2AsO_4^-$-2[a]	1.712	1.724	1.776	1.740	3.376	3.377	68.9
TiO_2–$H_2AsO_4^-$-3[a]	1.839	1.769	1.768	1.641	3.599	–	47.1
TiO_2–$HAsO_4^{2-}$-1[b]	1.755	1.757	1.796	1.672	3.454	3.450	60.6
TiO_2–$HAsO_4^{2-}$-2[b]	1.750	1.754	1.673	1.817	3.368	3.309	60.0
TiO_2–AsO_4^{3-}-1[c]	1.774	1.774	1.719	1.711	3.437	3.434	65.3
TiO_2–AsO_4^{3-}-2[c]	1.789	1.730	1.729	1.714	3.464	–	58.5

[a] At acidic pH condition.
[b] At neutral pH condition.
[c] At alkaline pH condition.

Figs. 6 and 7 and Tables 2 and 3 (A more detail report about the calculation results are in the appendix such as Figs. 4s–9s and Tables 1s–6s). In addition, the adsorptions of other relative species are also simulated such as water (24.6, 12.3 and 15.4 kcal mol^{-1}, respectively for the acidic, the neutral and the alkaline conditions), OH^- ion (66.1 and 49.3 kcal mol^{-1}, respectively for the neutral and the alkaline conditions), *etc.*

It is clear that the adsorption energies can fit with some results from the cluster model, such as in Table 3 the E_{ads} 69.8 and 68.9 kcal mol^{-1} of TiO_2–$HAsO_4^{2-}$-1[a] and TiO_2–$HAsO_4^{2-}$-2[a] qualitatively agree with 58.4 Kcal mol^{-1} of the As(V) BB complex at low pH [26], and the energy difference from 69.8 and 68.9 kcal mol^{-1} to 47.1 kcal mol^{-1} possesses the same trend from 16.7 to 9.2 Kcal mol^{-1} [27] for the BB and MM complexes. At the same time, our calculation results qualitatively agree with the experimental results from Jing et al. [6,30], Jegadeesan et al. [7] and Pan et al. [31] (see Table 7s in the appendix for detail). It should be noted that the calculation method used in the present paper such as the GGA exchange–correlation function possesses a trend of a little over estimate the bond distance which has been discussed in the paper of Zhang et al. [32].

Now we can explain the adsorption mechanisms. Based on the adsorption energies, the adsorption orders of As(III) and As(V) are AsO_3^{3-} > OH^- > $HAsO_3^{2-}$ > $H_2AsO_3^-$ > H_2O > H_3AsO_3 and AsO_4^{3-} > OH^- > $HAsO_4^{2-}$ > $H_2AsO_4^-$ > H_3AsO_4 > H_2O, respectively. Under acidic and neutral conditions, Eqs. (1)–(3) shows that H_3AsO_3 is the dominant species in aqueous solution whereas the adsorption ability of H_3AsO_3 is weaker than that of water, therefore the adsorption of As(III) is low at low pH range; the adsorption of As (III) increased from acidic to neutral and weak alkaline conditions, because $H_2AsO_3^-$ should appear on the surface, then the maximum adsorption appear at pH 8–9; $H_2AsO_3^-$ and $HAsO_3^{2-}$ cannot competitive with OH^- ion at high pH conditions, and only AsO_3^{3-} could compete with OH^- ion, therefore there is a minimum adsorption point at about pH 12 for As(III). Under acidic condition, Eqs. (4) and (5) show that $H_2AsO_4^-$ is the dominant As(V) species and its adsorption ability is stronger than that of water, therefore $H_2AsO_4^-$ should be the predominant species on the surface. The MM surface complex TiO_2–$H_2AsO_4^-$-3[a] can enhance the concentration of As (V) on the surface because it occupies only one surface Ti_{5c} site. At neutral and weak alkaline conditions, $HAsO_4^{2-}$ should present on the surface. It is interesting that even if many attempts have been made, we could not get a stable MM structure for $HAsO_4^{2-}$. One reason is that there would be only one H-bond between $HAsO_4^{2-}$ and surface O_{2c}, while two H-bonds can make the MM structure stable. The other reason is that the E_{ads} values of TiO_2–$HAsO_4^{2-}$-1[b] and TiO_2–$HAsO_4^{2-}$-2[b] are much higher than that of two waters. So $HAsO_4^{2-}$ should change to the BB types, even if its initial adsorption structure is a MM type. As a result, more BB type $HAsO_4^{2-}$ would make the adsorption density of As(V) lower. $HAsO_4^{2-}$ cannot competitive with OH^- ion at high pH conditions, and only AsO_4^{3-} can compete with OH^- ion, therefore there is a minimum adsorption point at about pH 12 for As(V). It is also significant to point out here that based on our calculation results there should be some negative charged arsenic species adsorped on the TiO_2 surface to make the total charge of the surface more negative. This conclusion agrees with the experimental results in Fig. 1 from Pena et al. [6] that the adsorption of As(V) and As(III) decreased the zeta potential of the TiO_2 particle, suggesting the formation of negatively charged inner-sphere surface complexes for both arsenic species.

4. Conclusion

To a deeper understanding of the pH effect for As(III) and As(V) adsorption behaviors on the TiO_2 anatase (1 0 1) surface, a broad pH range has been explored such as from pH 1 to pH 13.5. It is shown that the maximum adsorption of As(III) presents at pH 8 and its minimum adsorption presents at pH 12. The maximum and minimum adsorption pH values for As(V) are 4 and 12, respectively. The whole pH effect is crucial for arsenic adsorption and TiO_2 regeneration to improve arsenic remediation technology. Using DFT method, all the As(III) and As(V) solution species such as H_3AsO_3, $H_2AsO_3^-$, $HAsO_3^{2-}$, AsO_3^{3-}, and H_3AsO_4, $H_2AsO_4^-$, $HAsO_4^{2-}$, AsO_4^{3-} as well as water and OH^- ion are put onto the surface with various different possible attitudes to obtain their adsorption geometries and adsorption energies. Based on the calculated adsorption energies, $H_2AsO_3^-$ should be the predominant As(III) species on the surface from acidic to weak basic pH conditions, AsO_3^{3-} would be the predominant species at pH higher than 12. For As(V), $H_2AsO_4^-$ would present at acidic pH conditions, $HAsO_4^{2-}$ would present at neutral and weak basic pH conditions, AsO_4^{3-} would present at high pH conditions.

Acknowledgement

We thank GDUT high performance center for calculation support, and this work is supported by the National Natural Science Foundation of China (20803014, 21173022, 21373104) and the 211 funding program of Guangdong Province.

Appendix A. Supplementary material

The long time adsorption curve at pH 1 and pH 13.5; Simple sketches for the cluster model and the periodic slab model; The detail calculated results of As(III) and As(V) on TiO_2 anatase (1 0 1) surfaces; A comparison of the arsenic structures on the TiO_2 surfaces by EXAFS method. This material is available free of charge via the Internet at http://www.sciencedirect.com/.

Supplementary data associated with this article can be found, in the online version, at http://dx.doi.org/10.1016/j.jcis.2015.10.018.

References

[1] X. Meng, M. Dadachov, G.P. Korfiatis, C. Christodoulatos, Methods of preparing a surface-activated titanium oxide product and of using same in water treatment processes, U.S. patent, 2005,6,919,029.
[2] X. Guan, J. Du, X. Meng, Y. Sun, B. Sun, Q. Hu, Application of titanium dioxide in arsenic removal from water: a review, J. Hazard. Mater. 215–216 (2012) 1–16.
[3] P.K. Dutta, A.K. Ray, V.K. Sharma, F.J. Millero, Adsorption of arsenate and arsenite on titanium dioxide suspensions, J. Colloid Interface Sci. 278 (2004) 270–275.
[4] S. Bang, M. Patel, L. Lippincott, X. Meng, Removal of arsenic from groundwater by granular titanium dioxide adsorbent, Chemosphere 60 (2005) 389–397.
[5] M.E. Pena, G.P. Korfiatis, M. Patel, L. Lippincott, X. Meng, Adsorption of As(V) and As(III) by nanocrystalline titanium dioxide, Water Res. 39 (2005) 2327–2337.
[6] M. Pena, X. Meng, G.P. Korfiatis, C. Jing, Adsorption mechanism of arsenic on nanocrystalline titanium dioxide, Environ. Sci. Technol. 40 (2006) 1257–1262.
[7] G. Jegadeesan, S.R. Al-Abed, V. Sundaram, H. Choi, K.G. Scheckel, D.D. Dionysiou, Arsenic sorption on TiO_2 nanoparticles: size and crystallinity effects, Water Res. 44 (2010) 965–973.
[8] D. Nabi, I. Aslam, I.A. Qazi, Evaluation of the adsorption potential of titanium dioxide nanoparticles for arsenic removal, J. Environ. Sci. 21 (2009) 402–408.
[9] V.K. Sharma, M. Sohn, Aquatic arsenic: toxicity, speciation, transformations, and remediation, Environ. Int. 35 (2009) 743–759.
[10] S. Goldberg, C.T. Johnston, Mechanisms of arsenic adsorption on amorphous oxides evaluated using macroscopic measurements, vibrational spectroscopy, and surface complexation modeling, J. Colloid Interface Sci. 234 (2001) 204–216.
[11] J. Li, Y. Yu, Q. Chen, J. Li, D. Xu, Controllable synthesis of TiO_2 single crystals with tunable shapes using ammonium-exchanged titanate nanowires as precursors, Cryst. Growth Des. 10 (2010) 2111–2115.
[12] R.K. Dhar, Y. Zheng, J. Rubenstone, A. van Geen, A rapid colorimetric method for measuring arsenic concentrations in groundwater, Anal. Chim. Acta 526 (2004) 203–209.
[13] Z. Wei, S. Zhang, Z. Pan, Y. Liu, Theoretical studies of arsenite adsorption and its oxidation mechanism on a perfect TiO_2 anatase (101) surface, Appl. Surf. Sci. 258 (2011) 1192–1198.
[14] N.A. Benedek, I.K. Snook, K. Latham, I. Yarovsky, Application of numerical basis sets to hydrogen bonded systems: a density functional theory study, J. Chem. Phys. 122 (2005) 144102.
[15] J.P. Perdew, Y. Wang, Accurate and simple analytic representation of the electron-gas correlation energy, Phys. Rev. B 45 (1992) 13244–13249.
[16] V. Milman, M.C. Payne, V. Heine, R.J. Needs, J.S. Lin, M.H. Lee, Free energy and entropy of diffusion by *ab initio* molecular dynamics: alkali ions in silicon, Phys. Rev. Lett. 70 (1993) 2928–2931.
[17] M. Hakala, M.J. Puska, R.M. Nieminen, First-principles calculations of interstitial boron in silicon, Phys. Rev. B 61 (2000) 8155–8161.
[18] B. Delley, The conductor-like screening model for polymers and surfaces, Mol. Simul. 32 (2006) 117–123.
[19] A. Klamt, G. Schüürmann, COSMO: a new approach to dielectric screening in solvents with explicit expressions for the screening energy and its gradient, J. Chem. Soc., Perkin Trans. 2 (1993) 799–805.
[20] B. Delley, An all-electron numerical method for solving the local density functional for polyatomic molecules, J. Chem. Phys. 92 (1990) 508–517.
[21] B. Delley, Fast calculation of electrostatics in crystals and large molecules, J. Phys. Chem. 100 (1996) 6107–6110.
[22] B. Delley, From molecules to solids with the DMol3 approach, J. Chem. Phys. 113 (2000) 7756–7764.
[23] C.I. Sainz-Diaz, V. Timon, V. Botella, A. Hernandez-Laguna, Isomorphous substitution effect on the vibration frequencies of hydroxyl groups in molecular cluster models of the clay octahedral sheet, Am. Miner. 85 (2000) 1038–1045.
[24] A.C.Q. Ladeira, V.S.T. Ciminelli, H.A. Duarte, M.C.M. Alves, A.Y. Ramos, Mechanism of anion retention from EXAFS and density functional calculations: arsenic(V) adsorbed on gibbsite, Geochim. Cosmochim. Acta 65 (2001) 1211–1217.
[25] A. Vittadini, A. Selloni, F.P. Rotzinger, M. Gratzel, Structure and energetics of water adsorbed at TiO_2 anatase (101) and (001) surfaces, Phys. Rev. Lett. 81 (1998) 2954–2957.
[26] G. He, M. Zhang, G. Pan, Influence of pH on initial concentration effect of arsenate adsorption on TiO_2 surfaces: thermodynamic, DFT, and EXAFS interpretations, J. Phys. Chem. C 113 (2009) 21679–21686.
[27] G. He, G. Pan, M. Zhang, Studies on the reaction pathway of arsenate adsorption at water-TiO_2 interfaces using density functional theory, J. Colloid Interface Sci. 364 (2011) 476–481.
[28] L. Yu, Y. Liu, Z.G. Wei, G.Q. Diao, M. Sun, Q. Yu, Density functional theory calculations of arsenic(III) structures on perfect TiO_2 anatase (101) surface, Adv. Mater. Res. 233–235 (2011) 491–494.
[29] Z.G. Wei, Y.D. Zou, H.X. Zeng, X.C. Zhong, Z.J. Cheng, S.G. Xie, Density functional theory calculations of arsenic(V) structures on perfect TiO_2 anatase (101) surface, Adv. Mater. Res. 233–235 (2011) 495–498.
[30] C. Jing, S. Liu, M. Patel, X. Meng, Arsenic leachability in water treatment adsorbents, Environ. Sci. Technol. 39 (2005) 5481–5487.
[31] G. He, G. Pan, M. Zhang, XANES analysis of spectral properties and structures of arsenate adsorption on TiO(2) surfaces, J. Synchrotron Radiat. 19 (2012) 394–399.
[32] N. Zhang, P. Blowers, J. Farrell, Evaluation of density functional theory methods for studying chemisorption of arsenite on ferric hydroxides, Environ. Sci. Technol. 39 (2005) 4816–4822.